Anal. Bioanal. Electrochem., Vol. 14, No. 9, 2022, 818-836

Analytical & Bioanalytical Electrochemistry

2022 by CEE
www.abechem.com

Full Paper

A Cyanopyran Derivative for Preventing Corrosion of Pipeline Material Used in The Oil and Gas Industry

J. Saranya,[1,*] N. Anusuya,[2] F. Benhiba,[3,4] I. Warad,[5] and A. Zarrouk[3,*]

[1]*Department of Humanities and Sciences, Gokaraju Rangaraju Institute of Engineering and Technology, Hyderabad, Telangana, India*
[2]*Department of Chemistry, PSGR Krishnammal College for Women, Coimbatore, TamilNadu, India*
[3]*Laboratory of Materials, Nanotechnology, and Environment, Faculty of Sciences, Mohammed V University in Rabat, Av. Ibn Battouta, P.O. Box. 1014 Agdal-Rabat, Morocco*
[4]*Laboratory of Advanced Materials and Process Engineering, Faculty of Sciences, Ibn Tofail University, P.O. Box. 133, 14000, Kenitra, Morocco*
[5]*Department of Chemistry, AN-Najah National University, P.O. Box 7, Nablus, Palestine*

*Corresponding Author, Tel.: +212537774261

E-Mails: jcsaranya.chem96@gmail.com (J. Saranya); azarrouk@gmail.com (A. Zarrouk)

Received: 9 July 2022 / Received in revised form: 30 August 2022 / Accepted: 31 August 2022 / Published online: 30 September 2022

Abstract- The present work deals with the corrosion inhibition mechanism of mild steel in 1 M H_2SO_4 employing the new carbonitrile derivative viz. 2-amino-4-(4-hydroxyphenyl)-6-(p-tolyl)-4H-pyran-3-carbonitrile (HCN). A such mechanism was elicited by means of the potentiodynamic polarization (PDP) and electrochemical impedance spectroscopy (EIS) techniques and weight loss (WL). The experimental results revealed maximal inhibition efficiency (IE) rates up to 92.4% in weight loss. WL measurement revealed a decrease in corrosion rate with increasing concentration of corrosion inhibitor and decreasing with increasing temperature up to 333 K. The Nyquist curves indicated that the corrosion inhibition was controlled by a charge transfer process whereas the PDP curves showed that the HCN behaved as a mixed-type corrosion inhibitor. The Langmuir isotherm was used to determine the adsorption thermodynamic parameters. Thermodynamic characteristics for activation and adsorption were determined and discussed. Adsorption free energy at 303 K (ΔG°_{ads}= -22.26 kJ mol^{-1} for HCN) indicated a combination of chemisorption and physisorption. The inhibitor

(HCN) formed a protective layer that acted as a barrier between the surface of the metal and the acid medium which was investigated through surface studies like Scanning Electron Microscopy (SEM) coupled with Energy dispersive X-ray analysis (EDS). The surface studies were in coincidence with weight loss and electrochemical studies. Density functional theory (DFT) was performed to support the experimental data in an aqueous medium using the basis set 6-311G(d,p). From the Mulliken population analysis, the adsorption sites have been studied and the results of DFT were steady with the experimental studies.

Keywords- Oil and gas; Mild steel corrosion; Potentiodynamic polarization; Langmuir; SEM/EDS; DFT

1. INTRODUCTION

Metallic materials are frequently used in almost all industries, also they are sensitive and become corrode when they expose to various atmospheres like water, oxygen, humidity, salt, acid, etc. This is because metals are stable thermodynamically in their ore form, when the pure form of metal is unstable thermodynamically exposed to the atmosphere, it is the natural process of a metal to form ores depending on the constituents present in the atmosphere. Prevention of metal towards corrosion not only saves the industries, and economic loss to the nation, but it also has an impact on the environment [1]. Mild steel (MS) is also called low carbon steel which has 0.05– 0.25% carbon and also MS is one of the Fe alloys which is most widely used in industries like batteries, boilers, petroleum and oil, electroplating, etc. These industries are frequently working in acid environments. So, effective materials are always a good choice to handle this acid medium that needs utmost care and thorough knowledge of engineering. Due to the existence of some anions like chlorine, sulfides, nitrates, cupric salts, ferric salts, etc. present in the acid/alkali environment or a great level of aeration intensifies the oxidizing power of the solution which leads to enhanced corrosion mutilation. For the purpose of removing rust from the metal, metal specimens must be submerged in an acidic solution, such as diluted hydrochloric acid or sulphuric acid, which removes scales and rust from the metal surface. This procedure is referred to as acid pickling [2]. Though, after the removal of rust, acid continues to stay that attacks the pickled metal, and makes it dissolve, hence, to stop the influence of acid on the metal surface, a corrosion inhibitor is needed. Though other corrosion prevention techniques like coatings, modifying the design, paints, cathodic protection methods, etc. are available, the usage of inhibitors is found to be an efficient method for preventing metal from acid corrosion.

Corrosion inhibitors offer an efficient, convenient, cheap, non-toxic, easily available, and also cover the metal surface through protonation followed by the adsorption process that controls the metal corrosion in the aggressive medium. Chemisorption and physisorption are the two modes of the adsorption process in which an inhibitor interacts with the metal for prevention. The former takes place through the sharing/transferring of charge from the corrosion inhibitor molecules to the metal surface and forms a complex co-ordinate bond

whereas the latter results from the electrostatic or weak interaction between metal and the inhibitor molecules. Both processes can occur in some cases simultaneously.

To keep the metal inactive against corrosion, organic corrosion inhibitors are one of the active solutions for this process. Corrosion researchers are regularly searching for efficient organic inhibitors which should be cheap, non-toxic, economical, and must dissolve in aqueous solutions to mitigate the corrosion in industries. Heterocyclic compounds with unsaturated bonds play a major role in preventing metals from acid corrosion. The efficiency of such inhibitors also depends on the functional groups like -NH_2, -OH, etc., and heteroatoms like S, O, and N present in their chemical structure [3-10]. Nitrogen-containing heterocyclic compounds like benzimidazoles, pyrazoles, pyrimidines, purines, triazoles, etc have already been reported and reviewed in the aggressive medium [11-18]. Oxygen-containing heterocyclic compounds like pyran derivatives possess pharmaceutical and other biological activities [19,20]. Consequently, there were recent investigations based on the synthesis of pyran derivatives and their utilization of them as corrosion inhibitors. The authors reported that these pyran derivatives showed a good inhibition performance in various aggressive mediums [21-26].

The primary innovation of our research is the examination of the anticorrosive effects of 2-amino-4-(4-hydroxyphenyl)-6-(p-tolyl)-4H-pyran-3-carbonitrile (HCN) as an ecologically friendly inhibitor for MS-corrosion in H_2SO_4 electrolyte. Thus, this work aims the study how the cyanopyran derivative (HCN) influences the prevention of mild steel from acid corrosion through weight loss, electrochemical, and surface studies like SEM-EDS. In the aqueous phase, quantum chemical calculations were also carried out to determine the energy state and electronic structure of the inhibitor molecule. The results of experimental studies were consistent with the theoretical studies.

2. EXPERIMENTAL METHODS

2.1. Inhibitor Synthesis

Acetophenone (0.01 mol), 4-hydroxy-3,5-dimethoxybenzaladehyde (0.01 mol), and dry ethanol (20 mL) were mixed with the addition of NaOH (0.5 g) at 0 ˚C. The contents were stirred for about 360 minutes at room temperature. Then the mixture was decanted into ice-cold water and dil. HCl was added to maintain the pH between 3 and 4. The chalcone was obtained and it was filtered and recrystallized in anhydrous ethanol. Using an ultrasonic bath sonicator, an equimolar mixture of prepared chalcone in the above process and malononitrile were irradiated in the presence of pyridine for about 30 minutes. The obtained solid was added to cold water, the product was filtered and recrystallized from ethanol [27]. The HCN

compound was characterized by FTIR spectra using IR Affinity1 spectrometer (Shimadzu) and ^{13}C NMR spectra were recorded (Brucker, DPX-400 model – DMSO (solvent)).

2.2. Materials used for corrosion assessment

The MS specimens were rubbed with abrasive papers to get a very polished surface, degreased with acetone, and then air-dried. The composition of the MS, the abrasive paper used in the polishing and the procedure have been collected in Table 1.

Table 1. The composition of the MS, the abrasive paper used in the polishing and the procedure

(%) Composition of cold rolled MS	Certain elements like C- 0.084; Cr-0.022; Mo-0.011; Ni-0.013 & Fe-99.32
Dimension	3×1× 0.08 cm (weight loss (WL) & SEM-EDS studies) & 0.785 cm^2 (cylindrical rod for electrochemical studies)
Abrasive papers	1/0, 2/0, 3/0, and 4/0
Corrosive medium	1 M H_2SO_4
Chemicals	Purchased from Sigma Aldrich
Procedure	ASTM standard G31-72

2.3. Weight loss studies

The formulas described in the literature were utilized to compute characteristics like inhibitory efficiency (IE percent) and surface coverage (θ) [12]. The inhibition efficiency and corrosion rate from WL studies were calculated using the formulae,

$$\text{Inhibition efficiency (IE \%)} = \frac{(W_b - W_{inh})}{W_b} \times 100 \quad (1)$$

where W_b = WL without inhibitor; W_{inh} = WL with inhibitor,

Similar procedures were followed for different temperature ranges i.e., 313, 323, and 333 ±1K with 2 mM inhibitor concentration using the thermostat. Activation parameters like E_a, ΔH*, and ΔS* for the corrosion process were calculated using the formula,

$$\log CR = \frac{-E_a}{2.303RT} + \log A \quad (2)$$

$$CR = \frac{RT}{Nh} \exp\frac{\Delta S^*}{R} \exp\frac{-\Delta H^*}{RT} \quad (3)$$

h-Planck's constant, N-Avogadro number, T-absolute temperature, R-molar gas constant.

2.4. Electrochemical studies

IVIUM Compactstat Potentiostat/Galvanostat was used to record the electrochemical measurements. MS In order to get a stable result, specimens were submerged for 30 minutes

during a stabilization phase before being collected for E_{ocp} measurements. For determining the impedance characteristics, corrosion potentials with frequency ranges of 10000 to 0.1 Hz and signal amplitudes of 10 mV were used. Both the imaginary and real parts (Z′ and Z″) were measured at various frequencies. After completing EIS investigations in the same cell, the potential range for the open circuit potential was chosen to be between -200 mV and +200 mV at a sweep rate of 0.5 mV/sec [28]. The inhibition efficiency was calculated using the formula,

$$\text{Inhibition efficiency (\%)} = \frac{R_{p(inh)} - R_p}{R_{p(inh)}} \times 100 \quad (4)$$

where R_p and $R_{p\,(inh)}$ are the polarization resistance obtained in the absence and presence of the inhibitor. The inhibition efficiency was calculated from i_{corr} using the formula,

$$\text{Inhibition efficiency (\%)} = \frac{i_{corr} - i_{corr\,(inh)}}{i_{corr}} \times 100 \quad (5)$$

where i_{corr} and $i_{corr(inh)}$ signifies the corrosion current density in the absence and presence of an inhibitor.

2.5. Surface examination study

SEM and EDS techniques have been performed to observe the surface changes in the presence of acid with and without the inhibitor. WL method was followed for investigating surface studies using the equipment XRD, Bruker D8 Advance.

2.6. Computational studies

Computational studies like quantum chemical calculations are widely implemented to study the organic molecules containing heterocyclic atoms/rings for corrosion studies. The geometrical optimization of the studied inhibitor molecule HCN for the protonated and non-protonated forms in the aqueous phase was studied using DFT with basis set B3LYP- 6-311G(d,p) executed in the G09W package [29-31]. The output was then used to determine the molecular characteristics, such as the energy of the highest occupied molecular orbital (E_{HOMO}), energy of the lowest unoccupied molecular orbital (E_{LUMO}), energy gap (ΔE), electronegativity (χ), global hardness (η), global electrophilicity index ((ω), and total energy (TE), in order to identify the reactive sites in the structure [32,33].

3. RESULTS AND DISCUSSION

3.1. Spectral details of the inhibitor

The yield and color of the synthesized inhibitor namely 2-Amino-4-(4-hydroxyphenyl)-6-(p-tolyl)-4H-pyran-3-carbonitrile (HCN) is 99% and yellowish-brown solid respectively. The melting point of HCN is 244 ºC. IR spectrum (γ/cm^{-1}): 3621.36 (-OH); 3467.32 (-NH_2);

2241.75 (-C≡N), ^{13}C NMR (300 MHz, DMSO solvent-d6) δ (ppm): 117.4 (-C≡N), 134.9 (C-OH), 56.3 (Aliphatic -CH_3), 91.6-159.5 (pyran ring) (Fig. 1).

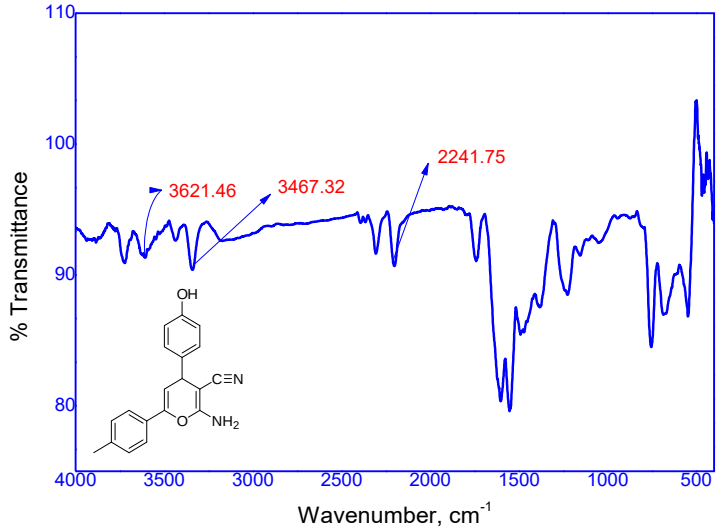

Fig. 1. FTIR Spectra of the inhibitor HCN

Table 2. Weight loss measurements

Temperature (K)	Concentration (mM)	Weight (mg/cm^2)	Surface area (θ)	Inhibition efficiency (%)
303±1	BLANK	0.0594	-	-
	0.1	0.0237	0.6010	60.1
	0.5	0.0178	0.7003	70.0
	1	0.0121	0.7963	79.6
	1.5	0.0084	0.8586	85.9
	2	0.0045	0.9242	92.4
313±1	BLANK	0.0687	-	-
	0.1	0.0331	0.5182	51.8
	0.5	0.0246	0.5859	58.6
	1	0.0167	0.7189	71.9
	1.5	0.0139	0.7660	76.6
	2	0.0087	0.8535	85.3
323±1	BLANK	0.1414	-	-
	0.1	0.0764	0.4597	46.0
	0.5	0.0596	0.5785	57.9
	1	0.0459	0.6754	67.5
	1.5	0.0388	0.7256	72.6
	2	0.0244	0.8274	82.7
333±1	BLANK	0.1833	-	-
	0.1	0.1094	0.4032	40.3
	0.5	0.0833	0.5456	54.6
	1	0.0653	0.6438	64.4
	1.5	0.0581	0.6830	68.3
	2	0.0334	0.8178	81.8

3.2. Weight loss method

The weight loss measurements were conducted three times under the same condition at 303±1K. Temperature and concentration of the inhibitor are the important parameters to fix the optimal condition for corrosion prevention of metals. The difference in the weight loss of the metal as a function of the inhibitor concentrations (0.1, 0.5, 1, 1.5, and 2 mM) in 1 M H_2SO_4 solution at varying temperatures (303, 313, 323, and 333±1 K) is displayed in Table 2. With an increase in inhibitor concentration, the MS inhibition efficiency steadily grew, declined, and fluctuated with temperature, respectively. The findings show that efficient inhibition of HCN is detected, which would be attributed to the protective layer generated at the interface between the MS and acid solution [34]. The inhibition efficiencies at higher temperatures were less compared to the lower temperature i.e., 303 K which specified that the inhibitor molecule was adsorbed through the electrostatic interactions, i.e., physical adsorption which are not existing at higher temperatures [35].

3.3. Activation parameters

The Arrhenius and transition plots were drawn to evaluate the parameters like activation energy, enthalpy, and entropy (equations 2,3) to obtain information about the metal dissolution process [36]. Table 3 showed the activation parameters for MS corrosion in acid solution at different temperatures (303 to 333 ±1 K). The E_a values (Arrhenius plot illustrated in Figure 2A) are greater for the inhibited solution than the blank solution which means it controls the corrosion rate for MS which indicates that the increased apparent activation energy for the inhibited acid solution/MS system can be taken as physical adsorption. Enthalpy (ΔH*) values in Table 3 and Figure 2B (Transition state plot) show that the steel dissolving phase is endothermic. The motivation behind removing its adsorption barriers on the steel surface is the change in negative value caused by a rise in HCN concentration. The negative entropy (ΔS*) values indicate the associative step rather than the dissociative and represent the disorderliness of the inhibitor/metal system [37].

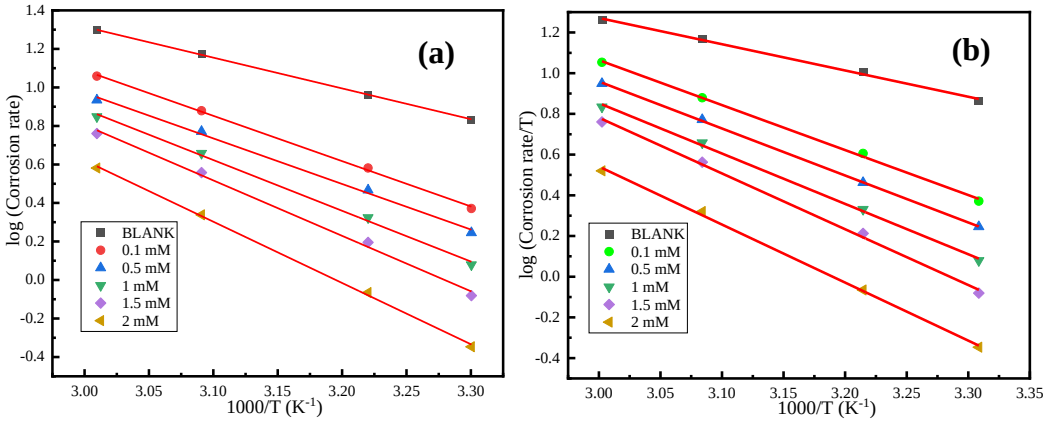

Figure 2. a) Arrhenius plot; b) Transition state plot

Table 3. Activation parameters

Concentration of the inhibitor	E_a kJ mol^{-1}	ΔH^* kJ mol^{-1}	$-\Delta S^*$ J $mol^{-1}K^{-1}$
Blank	27.25	31.68	90.25
0.1	45.45	42.81	41.05
0.5	46.30	43.66	40.68
1.0	50.82	48.18	29.11
1.5	57.39	54.75	10.16
2.0	59.04	56.40	9.32

3.4. Langmuir adsorption isotherm

The linear regression coefficient (R^2), which characterizes the adsorption isotherm model, is shown as a succession of straight lines that are getting closer to unity in Figure 3. Langmuir adsorption isotherm model was the most suitable fit for this HCN/metal/sulphuric acid system and is represented as follows

$$\frac{C}{\theta} = \frac{1}{K_{ads}} + C \quad (6)$$

where K_{ads}, C, and θ are, for the adsorption process, inhibitor concentration, and proportion of surface covered, respectively, equilibrium constants. The relationship between K_{ads} and the free energy of adsorption (ΔG°_{ads}) is given by the following expression

$$\Delta G^{\circ}_{ads} = -2.303 \times RT \times \log (55.5\ K) \quad (7)$$

The ΔG°_{ads} and K_{ads} values were calculated from equation 7 and presented in Table 4.

Figure 3 shows the Langmuir plot with the relation between C/θ and C at various temperatures. The high K_{ads} values specify the strong adsorption of the inhibitor HCN on the MS substrate and henceforth a better inhibition performance which is ascribed to the π-electrons present in the chemical structure of the inhibitor HCN. The negative values of ΔG°_{ads} give information about the spontaneity of the inhibitor HCN adsorption on the MS surface and also the nature of the adsorption process i.e., either physisorption or chemisorption [38].

Table 4. Langmuir adsorption parameters at 303 to 333 ±1 K

Temperature	R^2	Slope	K_{ads} mol lt^{-1}	$-\Delta G^{\circ}_{ads}$ kJ mol^{-1}
303 ±1 K	0.9984	1.05	144.44	22.26
313 ±1 K	0.9989	1.13	204.43	24.30
323 ±1 K	0.9986	1.16	224.14	25.32
333 ±1 K	0.9995	1.22	272.06	26.65

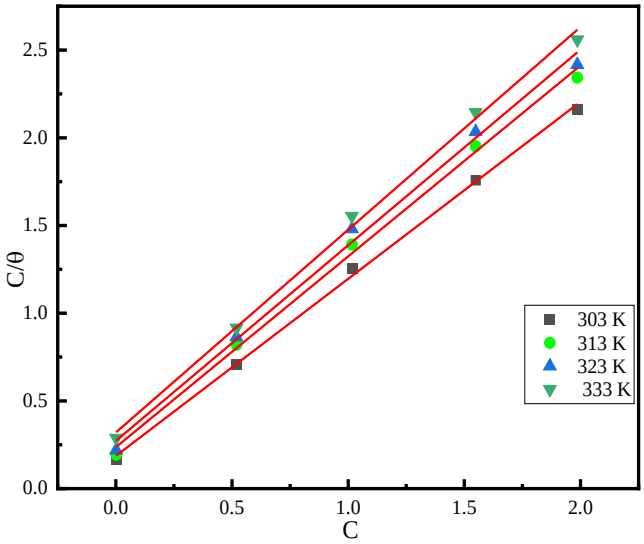

Figure 3. Langmuir plot

Generally, if the values of ΔG°_{ads} > −20 kJ mol^{-1} are attained, then the physisorption mechanism favors whereas if they are −40 kJ mol^{-1} or lower, then the chemisorption favors. Table 4 shows the ΔG°_{ads} values range from −22.26 to −26.65 kJ mol^{-1}, which is between −20 and −40 kJ mol^{-1}. Therefore, the adsorption process is a mix of chemisorption and physisorption.

3.5. Electrochemical impedance spectroscopy studies

EIS technique is used to know about the mechanism of the corrosion prevention process. The one-time constant equivalent circuit (Randle's) is used to fit and analyze the impedance data. Figure 4 shows the Nyquist and Bode&phase plots for the MS dipped in 1 M sulphuric acid with and without inhibitor at 303±1K. Table 5 shows the values of polarization resistance (R_p) and double-layer capacitance (C_{dl}). Nyquist plots show the increase in the diameter of the semicircle when the concentration of the inhibitor increases. This reveals that the inhibitive layer is formed at the MS/solution interface which indicates the decrease in C_{dl} values [39]. The drop in C_{dl} values reveals the displacement of water molecules and other ions by HCN molecules during adsorption, as well as the thickening of the adsorbed layer on the metal surface. When the concentration of the inhibitor is increased, an increase in R_p and a fall in C_{dl} readings indicate that a protective layer is forming on the MS surface, stopping the corrosion process [40,41].

Bode plots offer awareness of capacitive, resistive, and inductive behavior of the system at different frequencies and they can also be used for interpreting the EIS data along with the frequency of AC waves. Figures 4(a) and (c) represent the impedance and phase angle modulations with frequency (Bode plots) for MS corrosion in 1 M H_2SO_4 with and without inhibitor HCN. The charge transfer role in the metal dissolution process was revealed by the

presence of a single-phase angle plot [42]. Also, at intermediate frequencies, the maximum phase angles were seen and it has diverged from the ideal capacitive value of 90°, once more this feature highlights the non-ideal behavior of the MS/sulphuric acid system [43]. The maximum phase angle value and the phase angle shift towards lower frequency were found; these facts demonstrated that the addition of the inhibitor HCN and the inhibitor's barrier property reduced the rate of corrosion [44]. Moreover, the impedance value increased with an increase in the inhibitor concentration which was observed in Bode-impedance curves. In Bode plots (Figure 4b), we learned that the charge transfer process occurred at the MS/ acid interface which was revealed by only one phase maximum, showing only one relaxation procedure [45]. In other words, the decrease in surface roughness and inhomogeneity after adding HCN is due to the increase in the *n* value.

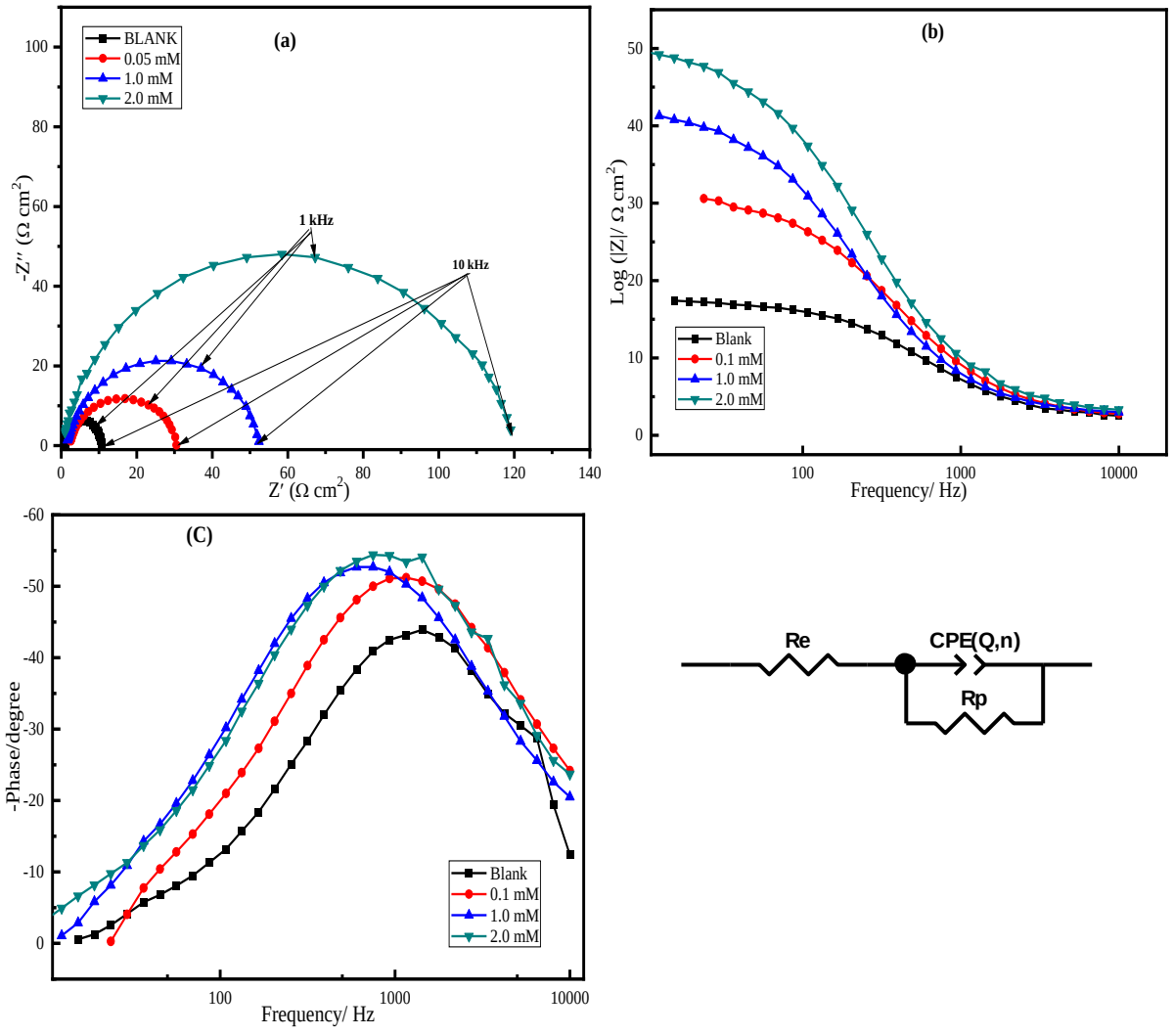

Figure 4. a) Nyquist; b) Bode; c) Phase diagrams in 0.5 M sulphuric acid solution with and without inhibitor; d) the circuit used to fit EIS spectra

Table 5. AC-impedance parameters for the selected concentrations of the inhibitor HCN at 303 ±1 K

Con. (ppm)	R_e (Ω cm^2)	R_p (Ω cm^2)	CPE		C_{dl} (μF cm^{-2})	$\chi\times10^{-3}$	Inhibition efficiency (%)
			$Q\times10^5$ (μF s^{n-1} cm^{-2})	n			
0.0	1.02±0.07	11.3±0.10	11.74	0.832±0.005	30.8	0.8	-
0.1	0.80±0.03	31.6±0.4	8.42	0.839±0.008	27.0	0.9	64.2
1.0	0.90±0.02	54.4±0.50	6.43	0.849±0.005	23.5	1.2	79.2
2.0	0.60±0.01	120.2±0.70	5.23	0.858±0.003	22.6	1.1	90.6

3.6. Potentiodynamic polarization studies

The inhibition effect of HCN with 3 different concentrations on the polarization of MS in 1 M sulphuric acid has been studied and is shown in Figure 5. It was observed from Table 6 that corrosion current density (i_{corr}) and corrosion rate were decreased substantially with the presence of inhibitor and the anodic, as well as the cathodic reaction of metal dissolution, got slowed. Regarding the E_{corr} value, it was seen in both Figure 5, the difference between the E_{corr} of acid solution without inhibitor and with inhibitor falls within 85 mV and approximately 51 mV was the maximum displacement in the direction of the anodic side. So, these assumptions propose that the inhibitor HCN does behave like a mixed type with a pro-anodic propensity. With the addition of an inhibitor, the Tafel slope values have been changed in the acid solution which also suggests the mixed-type behavior of HCN [46,47].

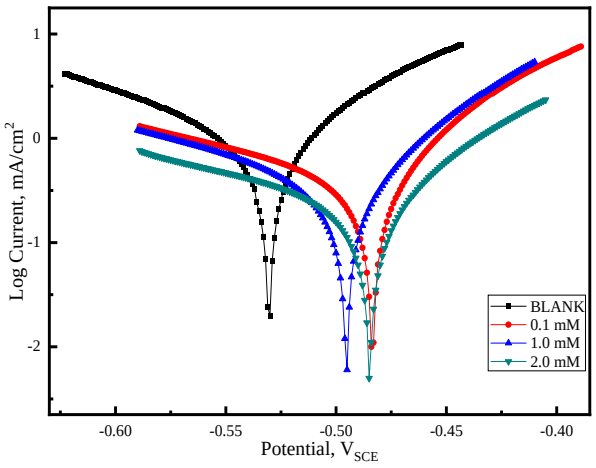

Figure 5. Tafel plots

Furthermore, the values of b_c/b_a are slightly altered by the addition of the tested inhibitor, and the change in the slope of the curve in the anode region is greater than that in the cathode region, indicating that the investigated inhibitor has a greater effect on the anode reaction in the H_2SO_4 environment. Generally speaking, there aren't many changes in the slope of the polarization curves, which shows that corrosion inhibitors can simply cover the metal surface

and lessen corrosion effects from the solution environment without modifying the corrosion mechanism. The inhibition effect of HCN was also confirmed by the results obtained from open circuit potential measurements, polarization, and impedance techniques. The comparable inhibition efficiencies obtained from all the techniques studied in the present work proved the efficiency of HCN towards the protection of MS in acid solution.

Table 6. Corrosion parameters obtained by the potentiodynamic polarization technique

Con. (mM)	Tafel slopes (mV/dec)		$-E_{corr}$ (mV/SCE)	i_{corr} ($\mu A\ cm^{-2}$)	Corrosion rate (mmpy)	Inhibition efficiency (%)
	b_a	b_c				
0.0	76	115	530.1	931.4	3.048	-
0.1	60	134	494.5	339.5	1.111	63.6
1.0	89	147	499.5	221.0	0.723	76.3
2.0	34	113	446.9	92.6	0.306	90.1

3.7. Surface studies

Surface studies like SEM-EDS were taken to examine the tendency of the inhibitor molecules (HCN) to protect the metal in acid solution. Here, in this study Figure 6a shows the SEM image of MS corroded in 1 M sulphuric acid solution where Figure 6b shows the SEM image of MS protected from acid solution due to the presence of inhibitor molecules HCN (2 mM concentration) on the surface of it. Thus, SEM images confirmed the presence of HCN molecules and their efficacy as a corrosion inhibitor. The cracks and pits were seen less in the presence of inhibitor (Figure 6b) whereas they were seen more in Figure 6a.

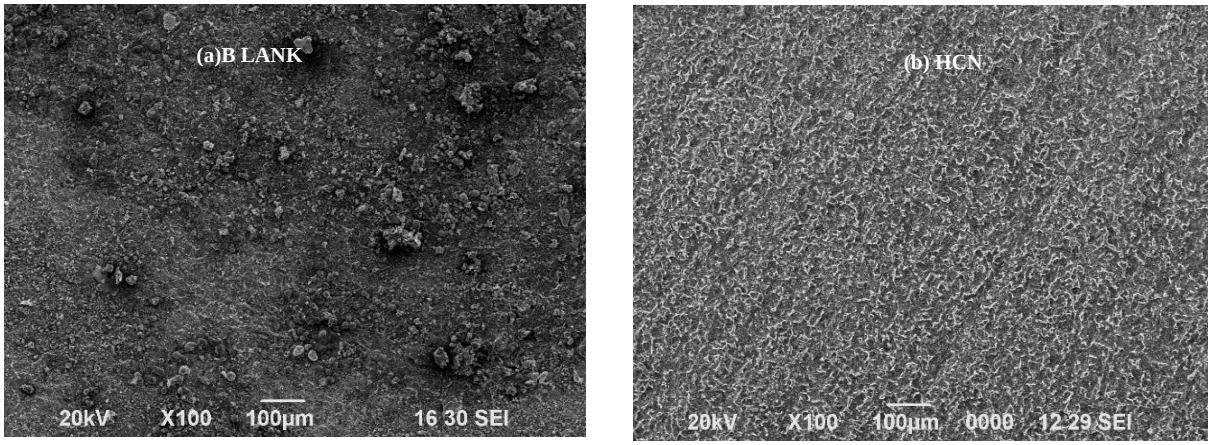

Figure 6. SEM for (a) Absence of inhibitor (b) Presence of inhibitor at 2 mM concentration

Figures 7a and 7b, respectively, display the EDS spectra of the MS in 1 M sulphuric acid in the absence and presence of a 2 mM concentration of HCN. Table 7 shows that the surface composition of Fe is increased and the additional peaks are also seen due to nitrogen and

oxygen in Figure 7b compared to Figure 7a indicates the presence of HCN adsorbed on the MS surface in acid solution. Both SEM and EDS studies proved that there is a mono-layer formation of the inhibitor molecule on the MS surface which prevents corrosion and also decreases surface roughness [48].

Table 7. Surface composition of mild steel after 3 hours of immersion in 1 M H_2SO_4 without and with the optimum concentration (2 mM) of the selected inhibitor HCN

Inhibitor	Element	Atomic weight (%)
BLANK	O	69.05
	Fe	40.95
HCN	C	18.58
	N	6.55
	O	9.56
	S	0.37
	Fe	64.94

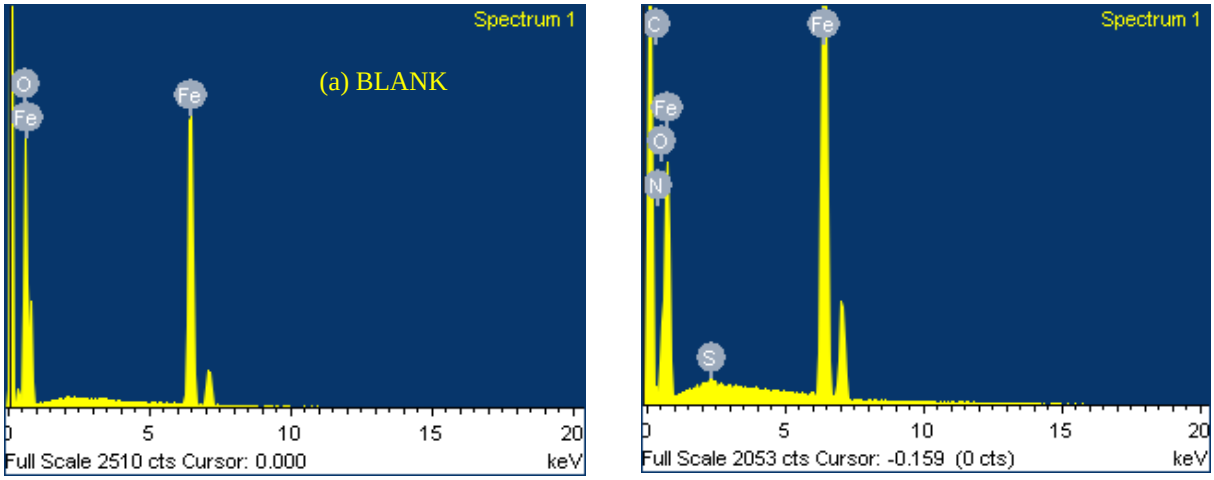

Figure 7. EDS analysis for (a) Absence of inhibitor and (b) Presence of inhibitor at 2 mM concentration

3.8. Quantum chemical studies

Quantum chemical methods give supportive methods to get information on the molecular property of the compounds. The data or parameters obtained from this method are used to compare the experimental data which are gained from weight loss, impedance, and polarization studies. In present days, inhibitors selection can be made possible by performing computational studies [49]. The parameters like E_{HOMO}, E_{LUMO} and band gap energy (ΔE), total energy, fractions of electrons transferred (ΔN), etc give valuable information about the molecule and with that information, the inhibition efficiency can be calculated and their order can also be calculated [50]. To get the data, molecular optimization is required using DFT with a suitable basis set. As presented in Figure 8, the GaussView 5.0 packet program was used [51] to build

up the input files and to plot the optimized structures of the frontier molecular orbitals (the highest occupied and lowest unoccupied molecular orbitals (HOMO and LUMO)) of the HCN neutral and protonated forms. The visual interlocking of the HOMO electron density distribution of the HCN neutral form shows that this distribution is mainly located almost on the majority of the studied structure except for the tolyl attached group. However, the LUMOs density distribution for the two forms studied is spread onto all structure. As regards the HOMO electron density distribution for the protonated form, it is quite obvious that this distribution is localized only on the 2-Amino-pyran-3-carbonitrile. Therefore, it is the only part that can donate electrons.

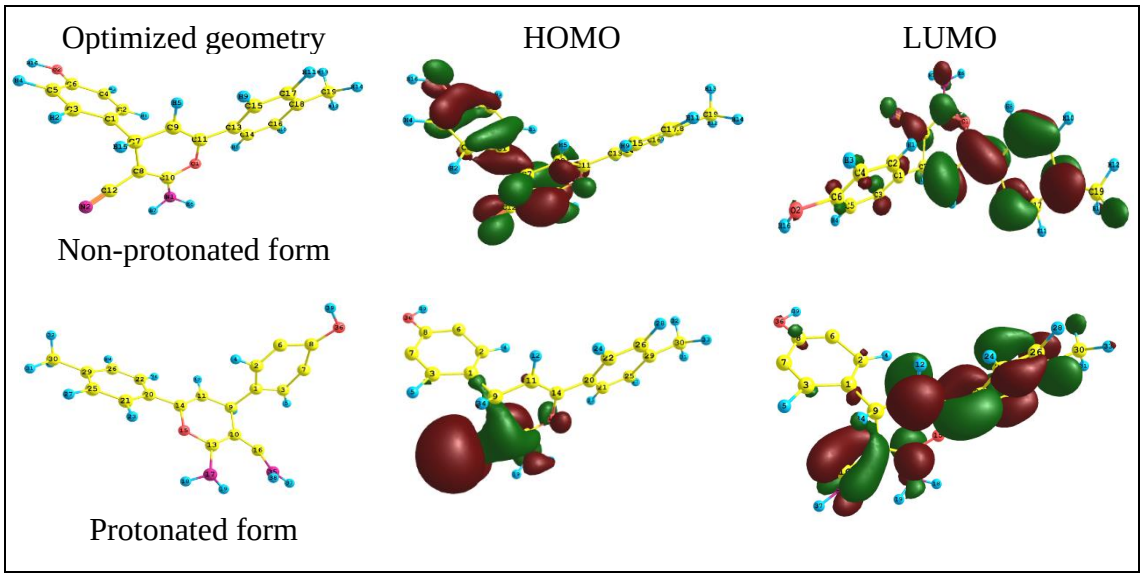

Figure 8. Optimized geometry, HOMO, and LUMO of the inhibitor HCN

The results obtained from the experimental data are consistent with the quantum chemical studies. It has been executed for both non-protonated and protonated forms of HCN and the values were depicted in Table 8. The data show that the high value of E_{HOMO} (-5.91 eV) for neutral form indicates that HCN is able to easily give electrons. However, the protonation of the molecule studied provokes a remarkable diminution of electron-donating power. The electron acceptor power experienced an increase when the molecule protonated (E_{LUMO} = -1.32 to -0.93 eV).

The smaller the value of ΔE, the lower will be the energy required to remove an electron from a molecule and the greater will be the reactivity and inhibition efficiency [52]. The smaller the ΔE is, the more reactive the HCN protonated (4.59 eV). Based on the hard and soft acid and Base (HSAB) theorem[53], the two interacting species should have identical/similar η/σ values. Consequently, as the softness (σ) increases and the hardness (η) value decreases, the interaction becomes more important. Therefore, the softener inhibitor, the one with a higher σ value and larger η value has a greater tendency to interact with the metal surface and vice versa.

According to our previous reports, it may be concluded that the molecular reactivity parameters (η, electronegativity (χ) and (σ) of the investigated inhibitor molecule are within the acceptable value, which means that the HCN protonated molecule may have a good anticorrosive property and can inhibit the metal from corrosion.

The estimated value of ΔN_{110} represents the number of electrons moved from the inhibitor to the empty sites on the iron surface [54]. It was already documented that the positive value of ΔN_{110} indicates a donor effect towards the unoccupied sites of the metal surface. In our case and as shown in Table 8, the neutral and protonated forms of HCN molecule have an electron donor capacity, which reinforces its adsorption on the study surface.

Table 8. Quantum chemical parameters of the neutral and protonated HCN

Calculated parameters	Non-protonated form	Protonated form
Total energy (amu)	-993.83	-994.4
Dipole moment (μ, debye)	4.56	3.75
E_{HOMO} (eV)	-5.91	-4.67
E_{LUMO} (eV)	-1.32	-0.93
Energy gap (ΔE, eV)	4.59	3.74
Ionization potential (I, eV)	5.91	4.67
Electron affinity (A, eV)	1.32	0.93
Hardness (η, eV)	2.30	1.87
Softness (σ, eV^{-1})	0.44	0.53
Electronegativity (χ, eV)	3.62	2.80
Fraction of electrons transferred (ΔN)	0.74	1.12

The possible adsorption sites for both forms of inhibitor HCN were studied through Mulliken atomic charges and they are shown in Figure 9. The atoms with more negative can easily donate the electrons to the metal surface and adsorption will be strong through donor-acceptor type interaction [55]. In addition, the atoms C15, C16 and O17 behave at the same time as electron donor and electron acceptor sites. HCN, it is clear that the protonated form bears several election acceptors sites, while the donor sites have undergone a noticeable decrease.

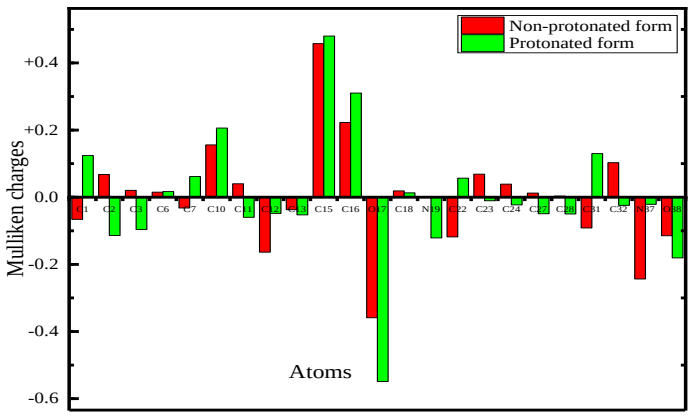

Figure 9. Mulliken atomic charges for the inhibitor HCN

3.9. Mechanism of corrosion inhibition

The oxidation reaction and hydrogen evolution are two critical processes that contribute to the corrosion process (reduction of hydrogen). Organic substances inhibit both of these two processes, preventing corrosion on the metal. The studied inhibitor showed mixed behavior according to the Tafel polarization method. So, the mechanism of the studied HCN inhibitor cannot be considered chemisorption or physisorption. In the first interpretation, chemisorption occurred owing to the presence of some electron-donating groups like -OH, $-NH_2$, $-CH_3$, π electrons, and pyran ring present in the HCN molecule [56]. These groups can cover the metallic surface regions of MS and provide electrons to the mild steel's vacant d orbitals. According to a second interpretation, physisorption occurred as a result of the attraction between inhibitors that protonated and charged the metal surface (MS surface has a positive charge as a result), and the negatively charged sulfate ions that initially adsorbed on the metal surface. Then, as a result of the electrostatic attraction between the positive metal and the negative inhibitor, inhibitor molecules formed a protective layer [57,58]. The adsorption of HCN was confirmed from SEM-EDS studies also. Quantum chemical calculations have also guaranteed the above-proposed mechanism with some variations.

4. CONCLUSIONS

2-amino-4-(4-hydroxyphenyl)-6-(p-tolyl)-4H-pyran-3-carbonitrile (HCN) was used as corrosion inhibitor for mild steel in H_2SO_4 solution. The inhibition efficiency of the HCN has been investigated by potentiodynamic polarization, electrochemical impedance spectroscopy and weight loss measurements. The adsorption behavior of HCN on MS in H_2SO_4 solution was examined using Langmuir adsorption isotherm and Gibb’s free energy. Scanning electron microscopy, Fourier transform infrared spectroscopy, and energy dispersive spectroscopy were used to characterize the MS and HCN. Maximum inhibition efficiency of 90.6% and 90.1% were recorded for potentiodynamic polarization and electrochemical impedance spectroscopy measurements respectively. Potentiodynamic polarization measurement revealed current density values to decrease with increasing HCN concentration while Tafel plot confirmed the inhibitor to be a mixed-type. Electrochemical impedance spectroscopy measurement revealed increase in polarization resistance values with increasing inhibitor concentration which affirmed the adsorption of inhibitor to be interface-type mechanism. The inhibition efficiency was shown to increase with increase in HCN concentration. Corrosion rate decreased as HCN concentration was increased temperature. A protective film forms on the mild steel surface to shield it from corrosion, according to surface analysis (SEM and EDS). Quantum chemical parameters provided the supportive data to correlate with the experimental data. All the results studied in this present study proved that the inhibitor is efficient towards metal corrosion in an acid medium even at a low concentration.

REFERENCES

[1] Z. Wang, L. Zhang, Z. Zhang, and M. Lu, Appl. Surf. Sci. 458 (2018) 686.

[2] M. BenSalah, R. Sabot, E. Triki, L. Dhouibi, P. Refait, and M. Jeannin, Corros. Sci. 86 (2014) 61.

[3] A. Kadhim, A. Al-Amiery, R. Alazawi, M. Al-Ghezi, R. Abass, Int. J. Corros. Scale Inhib. 10 (2021) 54.

[4] M.A. Hanoon, A. M. Resen, A. A. Al-Amiery, A. A. H. Kadhum, M. S. Takriff, Prog. Color Colorants Coat. 15 (2022) 21.

[5] F.G. Hashim, T.A. Salman, S.B. Al-Baghdadi, T. Gaaz, and A.A. Al-Amiery, Tribologia, 37 (2020) 45.

[6] A.M. Resen, M. Hanoon, R.D. Salim, A.A. Al-Amiery, L.M. Shaker, and A.A.H. Kadhum, Koroze a Ochrana Materialu. 64 (2020) 122.

[7] K. Tebbji, H. Oudda, B. Hammouti, M. Benkaddour, S.S. Al-Deyab, A. Aouniti and A. Ramdani, Res. Chem. Intermed. 37 (2011) 985.

[8] K. Tebbji, A. Aouniti, A. Attayibat, B. Hammouti, H. Oudda, M. Benkaddour and A. Nahle, Indian J. Chem. Technol. 18 (2011) 244.

[9] K. Tebbji, A. Aouniti, M. Benkaddour, H. Oudda, I. Bouabdallah, B. Hammouti and A. Ramdani, Prog. Org. Coat. 54 (2005) 170.

[10] K Tebbji, H Oudda, B Hammouti, M Benkaddour, F Malek and A Ramdani, Appl. Surf. Sci. 241 (2005) 326.

[11] C. Verma, L.O. Olasunkanmi, E.E. Ebenso, and M.A. Quraishi, I.B. Obot, J. Phys. Chem. C 120 (2016) 11598.

[12] C. Verma, L.O. Olasunkanmi, E.E. Ebenso, and M.A. Quraishi, RSC Adv. 6 (2016) 1.

[13] H. Tayebi, H. Bourazmi, B. Himmi, A. El Assyry, Y. Ramli, A. Zarrouk, A. Geunbour and B. Hammouti, Der Pharma Chem. 6 (2014) 220.

[14] A. Zarrouk, B. Hammouti, H. Zarrok, I. Warad and M. Bouachrine, Der Pharma Chem. 3 (2011) 263.

[15] A. Zarrouk, B. Hammouti, A. Dafali and H. Zarrok, Der Pharma Chem. 3 (2011) 266.

[16] H. Zarrok, R. Saddik, H. Oudda, B. Hammouti, A. El Midaoui, A. Zarrouk, N. Benchat and M. Ebn Touhami, Der Pharma Chem. 3 (5) (2011) 272.

[17] A. Ghazoui, R. Saddik, N. Benchat, B. Hammouti, M. Guenbour, A. Zarrouk and M. Ramdani, Der Pharma Chem. 4 (1) (2012) 352.

[18] H. Bendaha, A. Zarrouk, A. Aouniti, B. Hammouti, S. El Kadiri, R. Salghi and R. Touzani, Phys. Chem. News 64 (2012) 95.

[19] G. Zhang, Y. Zhang, J. Yan, R. Chen, S. Wang, Y. Ma, and R. Wang, J. Org. Chem. 77 (2012) 878.

[20] H. Gourdeau, L. Leblond, B. Hamelin, C. Desputeau, K. Dong, I. Kianicka, D. Custeau, C. Bourdeau, L. Geerts, S.X. Cai, J. Drewe, D. Labrecque, S. Kasibhatla, and B. Tseng, Mol. Cancer Ther. 3 (2004) 1375.

[21] D. K. Yadav, and M. A. Quraishi, Ind. Eng. Chem. Res. 51 (2012) 8194.

[22] J. Saranya, F. Benhiba, N. Anusuya, Ram Subbiah, A. Zarrouk, and S. Chitra, Colloids Surf. A: Physicochem. Eng. Asp. 603 (2020) 125231.

[23] M. Khattabi, F. Benhiba, S. Tabti, A. Djedouani, A. El Assyry, R. Touzani, I. Warad, H. Oudda, and A. Zarrouk, J. Mol. Struct. 1196 (2019) 231.

[24] A. Singh, K.R. Ansari, M.A. Quraishi, H. Lgaz, and Y. Lin, J. Alloys. Compd. 762 (2018) 347.

[25] J.N. Asegbeloyin, P. M. Ejikeme, L. O. Olasunkanmi, A. S. Adekunle, and E. E. Ebenso, Materials. 8 (2015) 2918.

[26] M. Yadav, L. Gope, N. Kumari, and P. Yadav, J. Mol. Liq. 216 (2016) 78.

[27] S. Debnath, V. Malla Reddy, S.Y. Manjunath, and M. Francis Saleshier, Int. J. Pharma. Sci. Nanotech. 3 (2010) 1153.

[28] M.V. Fiori-Bimbi, P.E. Alvarez, H. Vaca, C.A. Gervasi, Corros. Sci. 92 (2015) 192–199.

[29] M. El Faydy, F. Benhiba, B. Lakhrissi, M. Ebn Touhami, I. Warad, F. Bentiss, A. Zarrouk, J. Mol. Liq. 295 (2019) 111629.

[30] J. Peralta, F. Ogliaro, M. Bearpark, J. Heyd, E. Brothers, K. Kudin, V. Staroverov, R. Kobayashi, J. Normand, and K Raghavachari (2013) Gaussian 09, Revision D. 01, Gaussian, Inc.: Wallingford, CT.

[31] A. Zarrouk, B. Hammouti, A. Dafali, M. Bouachrine, H. Zarrok, S. Boukhris, and S.S. Al-Deyab, J. Saudi. Chem. Soc. 18 (2014) 450.

[32] R Hsissou, F. Benhiba, M. Khudhair, M. Berradi, A. Mahsoune, H. Oudda, A. El Harfi, I.B. Obot, and A. Zarrouk, J. King Saud. Univ. Sci. 32 (2020) 667.

[33] R. Nabah, F. Benhiba, Y. Ramli, M. Ouakki, M. Cherkaoui, H. Oudda, R. Touir, I. Warad, and A. Zarrouk, Anal. Bioanal. Electrochem. 10(10) (2018) 1375.

[34] S.A. Haddadi, E. Alibakhshi, G. Bahlakeh, B. Ramezanzadeh, and M. Mahdavian, J. Mol. Liq. 284 (2019) 682.

[35] N.A. Negm, S.M.I. Morsy, and M.M. Said, J. Surfactants. Deterg. 8 (2005) 95.

[36] O. Ghasemi, I. Danaee, G.R. Rashed, M. Rashvand Avei, and M.H. Maddahy, J. Cent. South Univ. 20 (2013) 301.

[37] A.S. Fouda, F.E. Heakal, and M.S. Radwan, J. Appl. Electrochem. 39 (2009) 391.

[38] Muhsen A. M. El-Haddad, A. Bahgat Radwan, Mostafa H. Sliem, Walid M. I. Hassan and Aboubakr M. Abdullah, Sci. Rep. 9 (2019) 3695

[39] Y. ELouadi, F. Abrigach, A. Bouyanzer, R. Touzani, O. Riant, B. ElMahi, A. El Assyry, S. Radi, A. Zarrouk and B. Hammouti, Der Pharma Chem. 7(8) (2015) 265.

[40] J. Zhao, and G. Chen, Electrochim. Acta 69 (2012) 247.

[41] G.A. Swetha, H.P. Sachin, A.M. Guruprasad, B.M. Prasanna, and K.H. Sudheer Kumar, J. Bio. Tribo. Corros. 4 (2018) 57.
[42] S. Abd El Wanees, A. Bahgat Radwan, M. A. Alsharif, and S.M. Abd El Haleem, Mater. Chem. Phys. 190 (2017) 79.
[43] D. Daoud, T. Douadi, S. Issaadi, and S. Chafaa, Corros. Sci. 79 (2014) 50.
[44] P. Singh, E.E. Ebenso, L.O. Olasunkanmi, I.B. Obot, and M.A. Quraishi, J. Phys. Chem. C 120 (2016) 3408.
[45] M. Srivasta, P. Tiwari, S. K. Srivastava, R. Prakash, and G. Ji, J. Mol. Liq. 236 (2017) 184.
[46] J. Saranya, P. Sounthari, K. Parameswari, and S. Chitra, Measurement. 77 (2016) 175.
[47] H. Zarrok, A. Zarrouk, R. Salghi, H. Oudda, B. Hammouti, M. Ebn Touhami, M. Bouachrinee and O.H. Pucci, Port. Electrochim. Acta 30 (2012) 405.
[48] M. Prajila, P. Rugmini Ammal, and Abraham Joseph, Egypt. J. Pet. 27 (2018) 467.
[49] A. Berrissoul, E. Loukili, N. Mechbal, F. Benhiba, A. Guenbour, B. Dikici, A. Zarrouk and A. Dafali, J. Colloid Interface Sci. 580 (2020) 740.
[50] R. Haldhar, D. Prasad, N. Mandal, F. Benhiba, I. Bahadur and O. Dagdag, Colloids Surf. A. 614 (2021) 126211.
[51] D. Roy, T.A. Keith, J.M. Millam, Current version: GaussView, version 6, Semichem Inc., Shawnee Mission. (2016).
[52] A. El yaktini, A. Lachiri, M. El Faydy, F. Benhiba, H. Zarrok, M. El Azzouzi, M. Zertoubi, M. Azzi, B. Lakhrissi and A. Zarrouk, Int. J. Corros. Scale Inhib.7 (2017) 609.
[53] F.H. Walters, J. Chem. Educ. 68 (1991) 29.
[54] Z. Rouifi, M. Rbaa, F. Benhiba, T. Laabaissi, H. Oudda, B. Lakhrissi, A. Guenbour, I. Warad and A. Zarrouk, J. Mol. Liq. 307 (2020) 112923.
[55] A.S. Fouda, S.M. Rashwan, S.M. Shaban, H.E. Ibrahim, and M.F. Elbhrawy, Egypt. J. Pet. 27 (3) (2018) 295.
[56] Parm Kumar, Shefali Dahiya, Raman Kumar, Suman Lata, Naveen Dahiya, and Suman Ahlawat, Ind. J. Chem. Tech. 24 (2017) 327.
[57] Ali Doner, Ramazan Solmaz, Muzaffer Ozcan, and Gulfeza Kardas, Corros. Sci. 53 (2011) 2902.
[58] Z. Rouifi, F. Benhiba, M. El Faydy, T. Laabaissi, H. Oudda, B. Lakhrissi, A. Guenbour, I. Warad, and A. Zarrouk, Ionics 50 (2021) 2267.